Planetary and Space Science 59 (2011) 2066–2074

Contents lists available at ScienceDirect

Planetary and Space Science

journal homepage: www.elsevier.com/locate/pss

The space environment of Mercury at the times of the second and third MESSENGER flybys

Daniel N. Baker [a,*], Dusan Odstrcil [b,c], Brian J. Anderson [d], C. Nick Arge [e], Mehdi Benna [f], George Gloeckler [g], Haje Korth [d], Leslie R. Mayer [h], Jim M. Raines [g], David Schriver [i], James A. Slavin [c], Sean C. Solomon [j], Pavel M. Trávníček [i,k], Thomas H. Zurbuchen [g]

[a] Laboratory for Atmospheric and Space Physics, University of Colorado, Boulder, CO 80303, USA
[b] Computational and Data Sciences, George Mason University, Fairfax, VA 22030, USA
[c] Heliophysics Science Division, NASA Goddard Space Flight Center, Greenbelt, MD 20771, USA
[d] The Johns Hopkins University Applied Physics Laboratory, Laurel, MD 20723, USA
[e] Air Force Research Laboratory, Kirtland Air Force Base, NM 87117-5776, USA
[f] Solar System Exploration Division, NASA Goddard Space Flight Center, Greenbelt, MD 20771, USA
[g] Department of Atmospheric, Oceanic and Space Sciences, University of Michigan, Ann Arbor, MI 48109, USA
[h] National Oceanic and Atmospheric Administration, Boulder, CO 80303, USA
[i] Institute of Geophysics and Planetary Physics, University of California, Los Angeles, CA 90095-1567, USA
[j] Department of Terrestrial Magnetism, Carnegie Institution of Washington, Washington, DC 20015, USA
[k] Astronomical Institute and Institute of Atmospheric Physics, ASCR, 14131 Prague, Czech Republic

ARTICLE INFO

Article history:
Received 8 July 2010
Received in revised form
17 December 2010
Accepted 27 January 2011
Available online 22 February 2011

Keywords:
Mercury
Solar wind
Interplanetary magnetic field
Magnetospheres
MESSENGER

ABSTRACT

The second and third flybys of Mercury by the MESSENGER spacecraft occurred, respectively, on 6 October 2008 and on 29 September 2009. In order to provide contextual information about the solar wind properties and the interplanetary magnetic field (IMF) near the planet at those times, we have used an empirical modeling technique combined with a numerical physics-based solar wind model. The Wang–Sheeley–Arge (WSA) method uses solar photospheric magnetic field observations (from Earth-based instruments) in order to estimate the inner heliospheric radial flow speed and radial magnetic field out to 21.5 solar radii from the Sun. This information is then used as input to the global numerical magnetohydrodynamic model, ENLIL, which calculates solar wind velocity, density, temperature, and magnetic field strength and polarity throughout the inner heliosphere. WSA-ENLIL calculations are presented for the several-week period encompassing the second and third flybys. This information, in conjunction with available MESSENGER data, aid in understanding the Mercury flyby observations and provide a basis for global magnetospheric modeling. We find that during both flybys, the solar wind conditions were very quiescent and would have provided only modest dynamic driving forces for Mercury's magnetospheric system.

1. Introduction

Recent years have seen a dramatic improvement in the comprehensive modeling of solar wind conditions throughout the inner heliosphere (e.g., Arge et al., 2004; Odstrcil et al., 2004). Much of this work has been motivated by the goal of providing forecasts of ambient solar wind conditions at Earth's location. The methods – which will be described in this paper – utilize photospheric magnetic field observations of the Sun from Earth-based instruments combined with empirical and physics-based (forward) numerical modeling tools. Present-day modeling is holding out new and improved prospects of "space weather" prediction capability.

In a previous paper (Baker et al., 2009) we described the solar wind conditions as modeled – and as observed – for the first Mercury planetary flyby by the MErcury Surface, Space ENvironment, GEochemistry, and Ranging (MESSENGER) spacecraft in January 2008. In that work we discussed the limitations of having only the single-point measurements at the MESSENGER location in the inner heliosphere. A much broader and more informative context is set for the spacecraft flyby results if one can provide a global inner heliospheric map of solar wind plasma and magnetic field conditions. From the previously noted state-of-the-art modeling efforts, one can have a clearer and more comprehensive picture of high-speed solar wind streams, corotating interaction regions, interplanetary magnetic field (IMF) sector boundaries,

* Corresponding author. Tel.: +1 303 492 4509; fax: +1 303 492 6444.
E-mail address: daniel.baker@lasp.colorado.edu (D.N. Baker).

0032-0633/$ - see front matter © 2011 Elsevier Ltd. All rights reserved.
doi:10.1016/j.pss.2011.01.018

and heliospheric current sheet properties throughout the inner solar system.

Since MESSENGER's first Mercury flyby (M1), the spacecraft has completed two further Mercury encounters. The second flyby (M2) on 6 October 2008 was fully successful from the standpoint of MESSENGER data collection (e.g., Slavin et al., 2009). During the third flyby (M3) on 29 September 2009, MESSENGER experienced a safe-hold anomaly shortly before the time of closest approach, and scientific data collection was stopped until the anomaly could be diagnosed and the spacecraft restored to operational mode. Nonetheless, remarkable new data were obtained on the M3 inbound trajectory (Slavin et al., 2010; Vervack et al., 2010).

In this paper, we first summarize our modeling technique and then review briefly our results for M1. The main goal of this paper is to provide detailed new results for M2 and M3. In each case, we use the available data from near 1 AU to test and validate the solar wind modeling for consistency and overall validity. In particular, *in situ* measurements from the Advanced Composition Explorer (ACE) and the Solar TErrestrial RElations Observatory (STEREO) pair of spacecraft provide the basis to assess our model results. We then compare the model results directly with available MESSENGER measurements. Finally, we discuss plans for modeling efforts as MESSENGER enters the Mercury orbital phase of the mission in March 2011.

2. Model description and prior results

As described by Baker et al. (2009), the Wang–Sheeley–Arge (WSA) model is a combined empirical and physics-based description of the global solar wind flow (Arge et al., 2004; Arge and Pizzo, 2000). It is widely used to predict the solar wind speed and IMF polarity at Earth (as well as other points in the inner heliosphere) and is an extension of the original Wang and Sheeley (1992) model. The model begins with ground-based observations of the solar surface magnetic field as input to a magnetostatic potential-field source surface (PFSS) model (Schatten et al., 1969) and yields estimates for the current sheet properties between 2.5 and 5 R_S (Fig. 1), where R_s is the solar radius. Updated solar field maps are used four times per day (6-h cadence). The outward flows in the corona, which are not explicitly contained in this PFSS formulation, are approximated by the imposition of radial field boundary conditions at the source surface and by an empirical relation that relates expansion factors to initial solar wind speeds at this point. This surface is a Sun-centered sphere of radius 2.5 R_s.

The photospheric field observations are the basic properties used to drive the computations. They serve as a key input to our coronal and solar wind models. Updated photospheric field synoptic maps (i.e., magnetic maps incremented regularly with new data) are constructed with magnetograms from the National Solar Observatory's Global Oscillation Network Group (GONG) system. The line-of-sight field measurements from these data sources are converted to the radial field component (see Arge et al., 2004). This radial field is the basis of our standard "forecast" version of the models. As described further below, in this paper we have used data from several different ground stations updated at a 6-h cadence and have scaled model parameters separately for the two encounters (M2 and M3).

From WSA results for the region near the Sun, an ideal magnetohydrodynamic (MHD) simulation, ENLIL (Odstrcil et al., 2004), is then used to model the solar wind flow outward to distances beyond 1 AU. The computational domain is a uniform grid occupying the sector of a sphere. The position of the inner boundary is set at 0.1 AU ($\approx 21.5\ R_S$), and the outer boundary is set at 1.1 AU. The meridional and azimuthal extents span 30–150° in heliospheric colatitude and 0–360° in longitude, respectively. The inner boundary lies in the supersonic flow region, near the outer field of view of the Large-Angle and Spectrometric Coronagraph (LASCO) C3 instrument on the Solar Heliospheric Observer (SOHO) spacecraft. The outer boundary at 1.1 AU allows comparison of simulated temporal profiles of solar wind properties at and near the Earth position with spacecraft measurements at ACE or other platforms (Odstrcil et al., 2004).

The combined WSA-ENLIL modeling is a specification of the solar wind flow speed, plasma density, solar wind mean plasma temperature, and magnetic field strength throughout the inner part of the heliosphere. A color representation of the radial flow speed (V_r) in the heliospheric equatorial plane computed for the entire inner heliosphere on 14 January 2008 is shown in Fig. 2a. The model results demonstrate that a broad solar wind stream region was present near the ecliptic plane during this time. The modeled solar wind speed enhancement (up to speeds of ~600 km/s) at ~1 AU was primarily in the longitude sector "trailing" the azimuthal location of the Earth (i.e., 0–90°E longitude). According to the model, the stream enveloped STEREO-B at the time of the snapshot but had not yet quite reached STEREO-A (Baker et al., 2009).

MESSENGER and Mercury were essentially collocated at the time shown in Fig. 2a and were subjected to nearly identical solar wind flow conditions. From a Mercury magnetospheric perspective, there was only a modest solar wind speed enhancement expected on the day of the flyby. The high-speed stream noted above would have passed over MESSENGER several days prior to the flyby with the highest-speed (600 km/s) stream features expected to rotate over the Mercury location several days earlier.

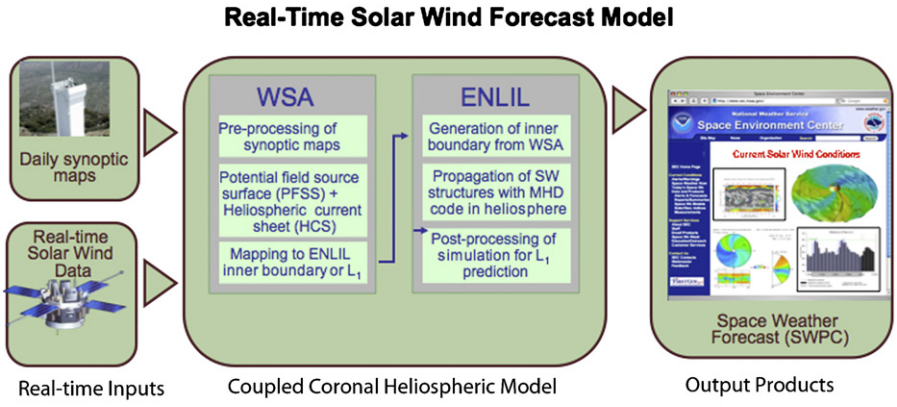

Fig. 1. Elements of the real-time coupled coronal-heliospheric model used in the present study. GONG data are used as input for the synoptic maps, and forecast outputs are given at the testbed site (http://swpc.noaa.gov/enlil/evolution). Definitions and abbreviations are described in the text.

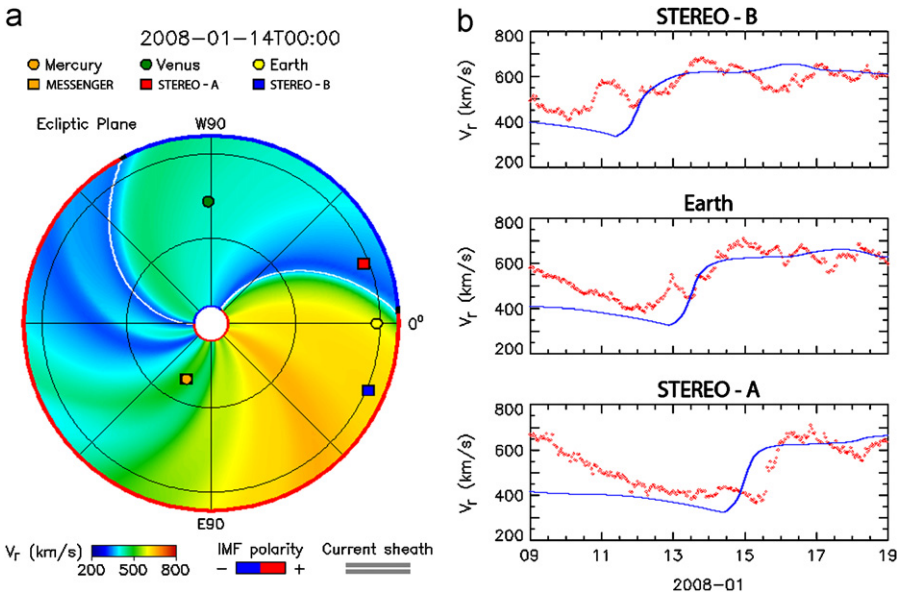

Fig. 2. (a) Modeled radial solar wind speed, viewed from the north ecliptic pole, obtained from the WSA-ENLIL model near the time of the first MESSENGER flyby of Mercury (14 January 2008). The scale for V_r is given by the color bar. The locations of Earth, STEREO-A, STEREO-B, Venus, Mercury, and the MESSENGER spacecraft are indicated by small colored dots. The inner domain of the model (where WSA is utilized) is denoted by the white central circle. The computational domain of the ENLIL simulation is shown by the colored area. The red-blue color coding along the edge of the outer boundary of computation shows the polarity of the IMF: red indicates IMF positive, or pointing away from the Sun, and blue indicates negative polarity with the IMF pointing toward the Sun. The white curves mark estimated IMF polarity sector boundaries near the equatorial plane. (b) Comparison of the WSW-ENLIL model results (blue curves) and the measured solar wind speeds (red symbols) for the 10-day period centered on M1: Top—STEREO-B; middle—ACE (Earth); bottom—STEREO-A.

Quiet conditions at Mercury on ~14 January 2008 (as suggested by the model) meant that the magnetosphere was relatively inactive during the spacecraft passage (see Baker et al., 2009).

A comparison of WSA-ENLIL solar wind speeds with concurrent measurements from ACE, STEREO-A, and STEREO-B is shown in Fig. 2b. The period of January 2008 was characterized by two broad solar wind streams (Baker et al., 2009) that were persistent and well-developed throughout the inner heliosphere. Earth (ACE) observations for that period show the onset of a high-speed stream on 5 January. Another high-speed stream commenced late on 12 January or early on 13 January. This second stream persisted for over a week at Earth, after which the solar wind speed eventually diminished to about 400 km/s by ~21 January. The WSA-ENLIL modeling results for a portion of this interval of time (9–19 January) are shown by the smooth blue lines in each panel of Fig. 2b. It is seen that most of the general features of the observed solar wind properties were emulated in the model. Certainly the solar wind stream seen near Earth commencing on 13 January was clearly captured by ENLIL. For this period, the density, temperature, and magnetic field strength values all were also reasonably well matched by the model (Baker et al., 2009). It was seen that the modeled solar wind speed rose a bit too early (by about one day) in the STEREO-A case. (The relative positions of the two STEREO spacecraft are shown in Fig. 2a.) Because of the general proximity of the STEREO-A and -B spacecraft to Earth, we see most of the same stream features at all three spacecraft. However, substantial timing differences were seen at the three locations.

Baker et al. (2009) emphasized that correct characterization of the solar wind stream properties at the three separated spatial locations (ACE, STEREO-A, and STEREO-B) is an important validation of the model's overall capabilities. The stream arrival times in the model were found to be reasonably similar to the observations at the three widely spaced observing points. This result indicates that the solar wind pattern in the inner heliosphere is essentially as predicted by the model and as illustrated in Fig. 2a. As was the case for the ACE comparisons with the model output, WSA-ENLIL also did a reasonable job of forecasting the solar wind and IMF data both ahead and behind the Earth locations as seen by the STEREO-A and -B spacecraft comparisons for the M1 period.

3. Flyby context: the deep solar minimum of 2007–2009

The three MESSENGER flybys of Mercury occurred during the most profound minimum of solar activity in the last century (e.g., de Toma et al., 2010). The period from late 2007 through most of 2009 had virtually no sunspot groups and very few solar active regions, and both solar wind flows and solar magnetic field weakened substantially during that interval (Smith and Balogh, 2008; McComas et al., 2008). This deep, extended minimum implied exceptionally quiescent conditions in the inner heliosphere, particularly (given our present interests) at the Mercury and MESSENGER locations.

One way of generally characterizing the in-ecliptic inner heliospheric solar wind conditions for the 2008–2009 period is to look at the average solar wind speed V_{sw} during this time (as continually registered by sensors near Earth). In Fig. 3, we present the daily solar wind speed from the "Omni" data set (http://omniweb.gsfc.nasa.gov/). A 7-day smoothing filter has been applied to the original daily average values. The data in Fig. 3 show quite clearly the overall diminution of the solar wind speed (on average) through 2008 and into 2009. Early in 2008 there were clear, well-developed solar wind streams with peak values of $V_{sw} > 600$ km/s. By late in 2008, the streams were still quite evident – with a persistent 27-day periodicity – but the peak solar wind speeds had dropped to just above 500 km/s. At the time of M2 (October 2008), the clear 27-day stream pattern was still evident. However, by 2009 the interplanetary stream structure had virtually gone away. For most of 2009, the solar wind speed at 1 AU barely rose above 400 km/s, and during the M3 period the

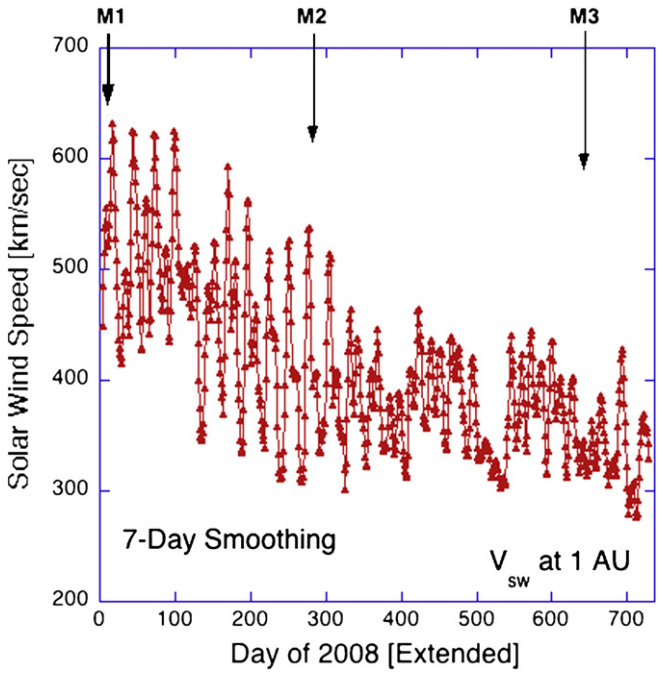

Fig. 3. Solar wind speeds measured by ACE near 1 AU for the period 2008–2009. Daily speed values have been smoothed with a 7-day averaging filter. The times of the three MESSENGER flybys of Mercury are indicated for reference.

speed was often near 300 km/s. Since these flow conditions would generally have obtained not only at Earth but also at Mercury's location (at slightly different times, of course), we would expect that solar wind driving of Mercury's magnetosphere would have been weak. This condition would have been especially true for the M3 period.

4. Modeling the second Mercury flyby

As noted above, the WSA model is a key component of the overall inner heliospheric description. WSA is routinely used by space weather forecasters to predict solar wind properties at 1 AU several days in advance. A recent improvement in the WSA approach is the Coronal hole Analysis Tool (CAT). This tool provides a quicker and easier way to assess the overall agreement between the observed coronal hole configuration on the Sun with that determined in the WSA model. The CAT plots indicate the magnetic neutral-line transitions in the photospheric field.

A display for 6 October 2008 is shown in Fig. 4. The image in Fig. 4b is the SOHO Extreme ultraviolet Imaging Telescope (EIT) image (19.5 nm wavelength) at 1248 UTC on 6 October. The CAT diagram in Fig. 4a shows the magnetic polarity and coronal hole structures that are estimated in the WSA model. One can see from the CAT portrayal (and from the EIT image) that there were relatively small coronal holes on portions of the visible Sun. Although the Sun had no major active regions during this period, the modest coronal hole regions (such as in the southern solar midlatitude region) would produce some solar wind stream structures.

The WSA results such as those derived using Fig. 4 form the basis for subsequently driving the ENLIL model. ENLIL then simulates three-dimensional evolution and dynamic solar wind stream interactions for the remaining inner heliosphere configuration. Fig. 5 shows the modeled values for the radial component of the solar wind velocity (V_r) and the solar wind density (N) in the equatorial heliospheric plane using the WSA-ENLIL combination. (Note that N is normalized to values at 1 AU.) Fig. 5a shows that Mercury (and MESSENGER) and Earth were almost perfectly aligned along the same radial line outward from the Sun on 6 October 2008. Whereas a slightly higher-speed ($V_{sw} > 500$ km/s) solar wind stream had passed over Mercury and Earth in the prior 3–4 days, by 6 October Mercury and MESSENGER were within much slower ($V_{sw} \sim 400$ km/s) flow. In Fig. 5b, it is seen that Mercury and Earth also were in low-density solar wind plasma on 6 October. It should be noted that the density was generally rising at this time ahead of the magnetic polarity reversal boundary that was just about to pass over Mercury.

The solar wind conditions modeled for the STEREO-A, Earth (ACE), and STEREO-B locations before, during, and after the time of M2 are shown in Fig. 6. From this composite figure, it is seen that WSA-ENLIL shows modeling agreement with the several spacecraft at 1 AU but also some obvious discrepancies. Fig. 6 shows that one difference at the three spacecraft locations is that the modeled peak speeds are not as large as those measured by ACE and the STEREO probes. However, overall the model results and the observations are in rather reasonable correspondence on stream onset timing. This agreement indicates that WSA-ENLIL provides a valid global representation of inner heliospheric stream patterns and therefore provides useful context at MESSENGER. We note that the average magnitudes of the solar wind densities and field strengths are quite similar to the model results in Fig. 6. However, the observed ranges of variations in the spacecraft data are again much larger than the model results would suggest. We also note that the temperature measurements are not well replicated (see the discussion of this aspect by Baker et al., 2009).

The solar wind profiles and IMF values that were calculated with the WSA-ENLIL model at the MESSENGER location from 29 September to 13 October 2008 are shown in Fig. 7. From the model results, we see that the time of MESSENGER's closest approach to the planet was, indeed, expected to be a period of very low solar wind speed ($V_{sw} \sim 360$ km/s) and only slightly increasing density ($N \sim 60$ cm^{-3}). The magnetic field strength was computed to be fairly steady throughout this entire period. The local IMF strength was estimated at $B \sim 15$ nT during the encounter period, according to the model.

The model results are compared with the *in situ* spacecraft measurements in Fig. 7 (panels a, c, and d). We plot the nearly continuous MESSENGER Magnetometer data (Anderson et al., 2008) over the model curve of B in panel d. These comparisons show that the model values are in quite good agreement with the measured values from MESSENGER throughout most of the interval. Near the end of the period, the field magnitude measured by MESSENGER increased considerably, and the model values track this increase reasonably well. Hence, in broad terms, the ENLIL and MESSENGER magnetic field trends are quite similar, especially before the flyby. Any differences in the magnitude of the modeled IMF from the observations is likely an issue with the observed photospheric fields (used to drive the model) being too small. There is an important and unresolved controversy about this topic in the solar and modeling community: In essence, the observed open flux is greater than the modeled open flux. As noted in Section 2 above, we have used here an improved version of the WSA model inputs (rather than the standard GONG forecast values). This choice results in good data–model closure in this case.

Because of the location of the plasma analyzer (Raines et al., this issue) on the MESSENGER spacecraft and because of spacecraft pointing constraints, we do not have continuous or complete MESSENGER measurements of the solar wind. During limited intervals throughout the period covered in Fig. 7, however, it was possible to obtain a sufficient fraction of the solar wind

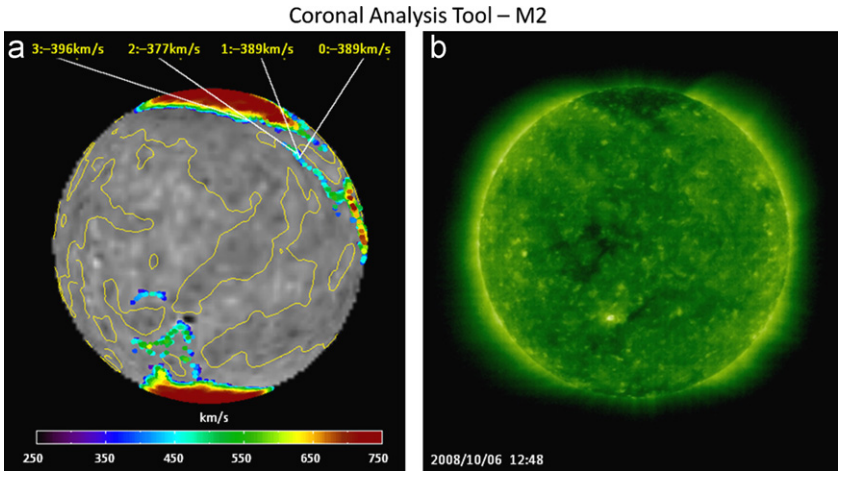

Fig. 4. (a) The Coronal hole Analysis Tool (CAT) representation for the time of the second MESSENGER flyby of Mercury (6 October 2008). (b) The SOHO/EIT image (19.5 nm wavelength) at 1248 UTC on 6 October 2008, for comparison with (a).

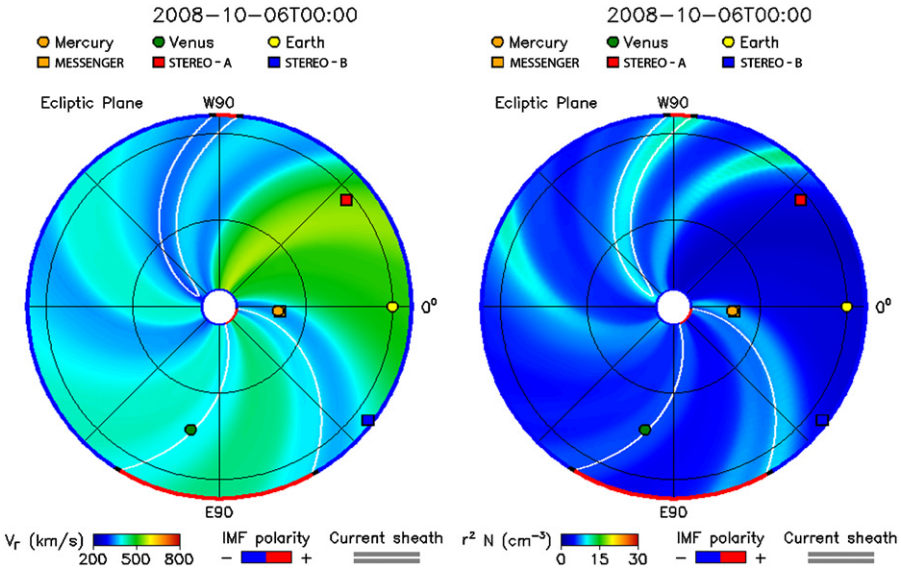

Fig. 5. (a) Similar to Fig. 2a but for M2 (6 October 2008). (b) Similar to (a) but showing the solar wind density in the inner heliosphere as modeled by WSA-ENLIL. The density color representation is scaled by squared solar distance $r2$ to the value at 1 AU.

distribution function to generate estimates of plasma parameters (particularly speed and temperature). Data for such intervals are plotted in red together with the corresponding model curves in blue. The MESSENGER speed estimates are close to the ENLIL calculations, and the inferred temperatures are higher than in the model. (Temperature modeling is a continuing challenge; see Baker et al., 2009.) Naturally, the measured solar wind parameters show more structure and higher time variability than the model, which would be expected given the slower (6-h) cadence of inputs (ground-based) and inherent spatial smoothing to the model calculations. (Note that WSA maps based on GONG data have 2.5° angular resolution, which translates into a temporal resolution of ~4.5 h.) Also, the solar wind is known to have a substantially increased variability on shorter temporal scales (Schwenn, 1990; Raines et al., this issue), which is also contributing to the differences in Fig. 7.

Derived parameters relevant to magnetospheric modeling of the Mercury system are provided in the bottom three panels of Fig. 7. The fifth panel shows the sonic Mach number (in blue) and the Alfven Mach number (in green). These values are pertinent to estimating the expected bow shock and magnetopause properties at Mercury (e.g., Slavin et al., 2008). The sixth panel shows our calculated values of the potential drop E_{drop} (in kilovolts) across the Mercury magnetosphere (see Baker et al., 2009). We have used the ENLIL model solar wind speed combined with the measured normal component of the magnetic field and a scaling distance of one Mercury radius (R_M=2440 km) to compute E_{drop}. Such estimates of potential drop provide an important measure of possible modes of particle acceleration that might occur within the Mercury magnetotail (e.g., Baker et al., 1986). The bottom panel shows the estimated solar wind dynamic pressure, P_{dyn}.

5. Modeling the third Mercury flyby

A CAT image set for the day of the third Mercury flyby (29 September 2009) is shown in Fig. 8a. In contrast to the situation at the time of M2, we can see from Fig. 8 that at the time of M3 there were two bright active regions on the visible disk of the Sun, and there was also a well-defined coronal hole in the northern solar hemisphere near the central meridian. These

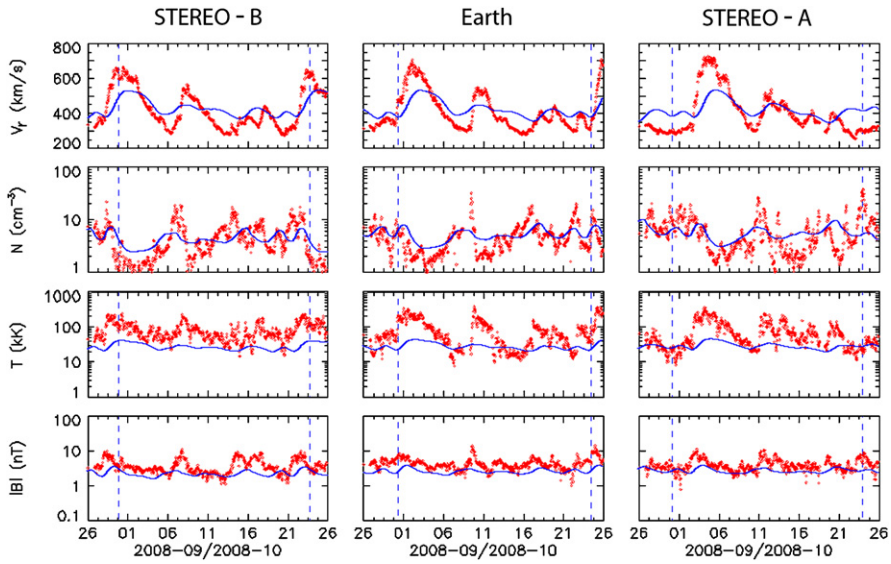

Fig. 6. Model and data comparisons for spacecraft near 1 AU for a period bracketing the time of M2 (6 October 2008). The top panel in each case shows solar wind speed. The second panel is density, and the third is solar wind temperature. The bottom panel in each case shows the modeled and observed values of magnetic field strength at STEREO-B (left), ACE (middle), and STEREO-A (right).

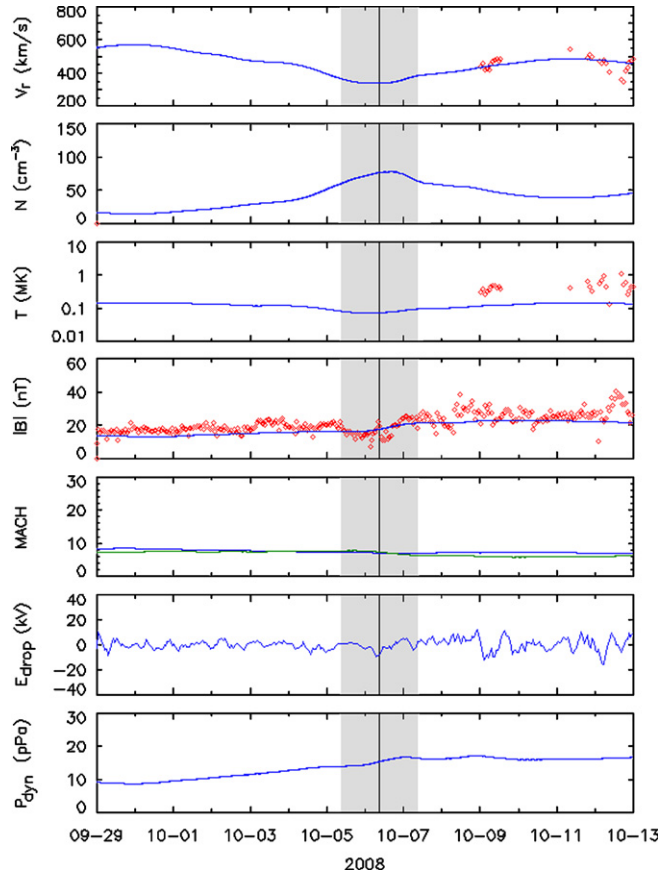

Fig. 7. Modeled solar wind parameters for the period 29 September to 13 October 2008. The shading in each panel shows the interval immediately surrounding M2 (5–7 October). The top three panels show, respectively, the solar wind speed, density, and temperature for this period. The fourth panel shows the calculated value of the IMF magnitude for the same interval of time. The red data points plotted in the first, third, and fourth panels show, for comparison, MESSENGER magnetic field and available plasma data (as described in the text) for the period. The bottom three panels show other (derived) quantities. The fifth panel shows the sonic and Alfvén Mach numbers. The sixth panel shows estimates of the cross-magnetospheric potential E_{drop} (see text), and the bottom panel shows dynamic pressure P_{dyn}.

features are captured well in the CAT image and, hence, in the WSA modeling.

A north polar perspective view of the equatorial model results from WSA-ENLIL (analogous to Fig. 5 above) for 29 September is shown in Fig. 9. For M3, we see that Mercury (and MESSENGER) was almost precisely on the same Archimedean spiral line as that threading the Earth's position (farther out in the heliosphere). This would, presumably, lead to quite good nominal magnetic connectivity between Mercury and Earth at that time. We note that this type of alignment can be used quite effectively, for example, in issuing space weather alerts for energetic solar particle events.

As shown in Fig. 9a, there was a strong and well-developed solar wind velocity stream some 90° in solar longitude ahead of Mercury (and Earth). A much weaker stream had just rotated past the Mercury and Earth longitudes as well. However, on this day of closest MESSENGER approach, the solar wind speed was modeled to be relatively low (and declining). Fig. 9b suggests that Mercury and MESSENGER were in an exceptionally low-density sector as well.

WSA-ENLIL model results for the M3 period are compared with *in situ* solar wind measurements for STEREO-A, ACE, and STEREO-B (in analogy with Fig. 6) in Fig. 10. Throughout the modeled interval, the measured speed, temperature, and IMF values were generally similar in their ranges to what was measured at the respective spacecraft. However, detailed features and specific peaks do not all line up at precisely the modeled times. Overall, the model and measurement results agree rather well, especially for the STEREO-B and Earth locations.

Model results and MESSENGER measurements are compared in Fig. 11 for a period (22 September–6 October 2009) bracketing M3. As was the case for Fig. 7, the model results are shown as smooth curves in each panel, and the available MESSENGER data are shown as red symbols. The model suggests that on 29 September Mercury was in a region of average solar wind speed region ($V_{sw}\sim$350–400 km/s) and modest density ($N\sim$50 cm^{-3}).

At the beginning of the interval (22–23 September), the MESSENGER plasma data agree well with the model results. (Note that prior to M3 the plasma investigation team had implemented several improved data acquisition and analysis strategies that yielded more complete observations than for prior flybys.)

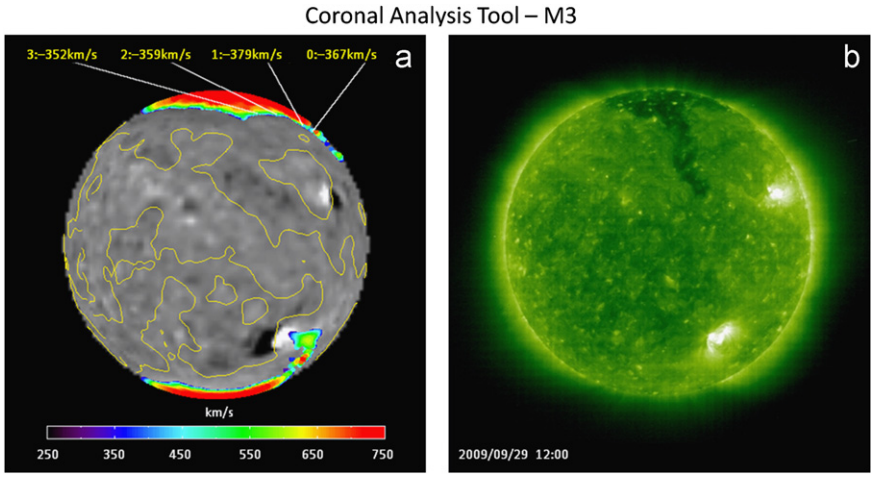

Fig. 8. Similar to Fig. 4 but for the time of M3 (29 September 2009).

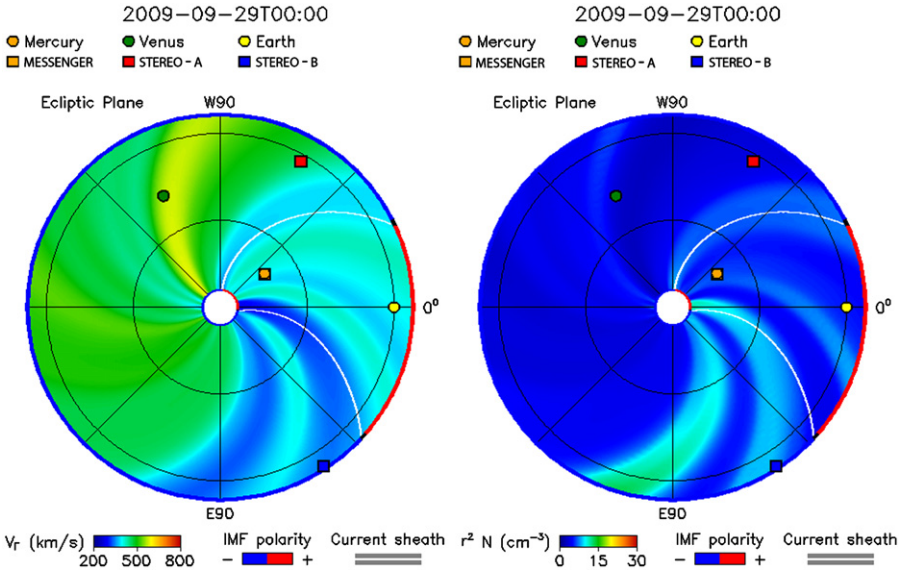

Fig. 9. Similar to Fig. 5 but for the time of M3 (29 September 2009).

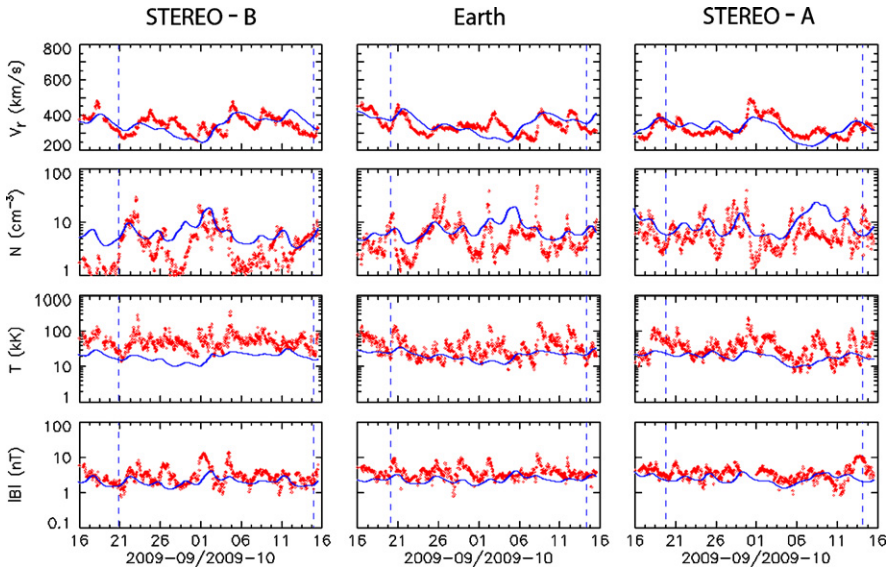

Fig. 10. Similar to Fig. 6 but for the M3 interval (16 September–15 October 2009).

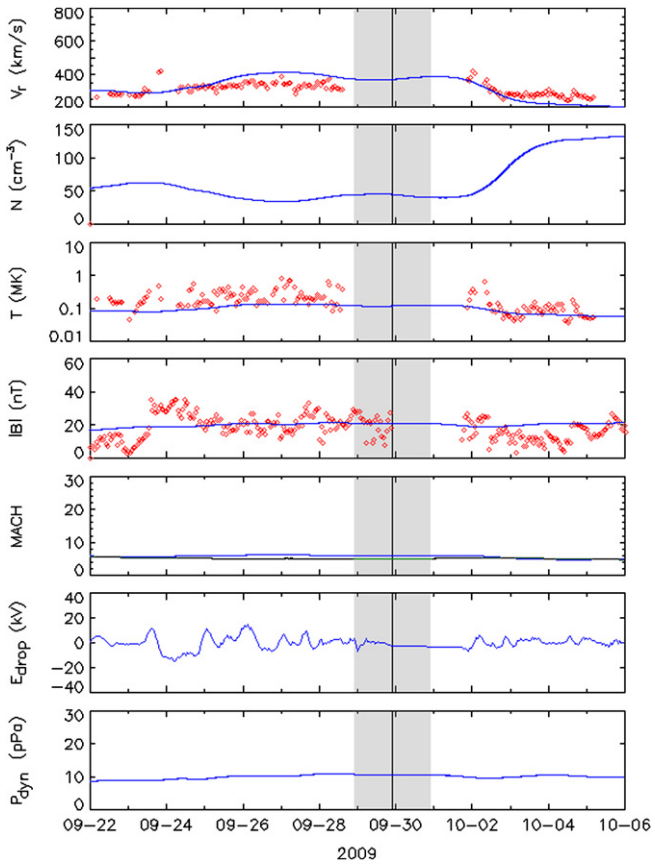

Fig. 11. Similar to Fig. 7 but for the M3 interval (22 September–6 October 2009).

However, the agreement for the magnetic field data is not as clear on 22–23 September. From 24 September to ~3 October, the magnetic field values at MESSENGER were quite similar to the modeled values. After the encounter, good plasma parameter agreement was again obtained. (As noted above, the MESSENGER spacecraft went into safe mode near closest approach on 29 September, and no data were available from then until near the end of 1 October.)

6. Discussion and conclusions

The combined WSA and ENLIL models provide important contextual information about the solar wind and IMF conditions in the inner heliosphere during the times surrounding the MESSENGER flybys of Mercury. Comparisons both before and after the times of closest approach tend to show that the MESSENGER field magnitudes were quite similar to the model results for most of the weeks-long intervals of comparison. Using more carefully chosen ground-based photospheric magnetic field maps rather than standard GONG forecast tools gives good field agreement at MESSENGER. Because of sensor location on the spacecraft, available MESSENGER solar wind plasma measurements, especially during M2, were of only limited utility for comparison with model outputs. However, the available MESSENGER solar wind speed data for M3 tend to agree remarkably well with the ENLIL results. The model results clearly show that Mercury's magnetosphere during both M2 and M3 was being subjected to extensive regions of low-speed, quiet solar wind. This information helps explain some of the magnetosphere properties that were sampled by MESSENGER sensors (Slavin et al., 2009, 2010).

The robust prediction of basic solar wind parameters provided by the techniques described here is also useful as an initial boundary condition in detailed simulations of the response of Mercury's magnetospheric system to the solar wind. Detailed simulations of Mercury's magnetosphere are carried out either using an MHD approach (Benna et al., 2010) or via a hybrid description of plasma that retains kinetic properties for ions but treats electrons as a massless fluid (Trávníček et al., 2007, 2009, 2010). Both MHD and hybrid simulations provide detailed three-dimensional models of the plasma environment around Mercury. These have proven to be useful for interpretation of MESSENGER's observations of Mercury's magnetic field by the Magnetometer instrument and were used further for particle tracing to model the circulation of heavy ions and electrons around Mercury.

Table 1
Summary of WSA-ENLIL solar wind modeling results for the three MESSENGER flybys.

Encounter	V_{sw} (km/s)	N (cm^{-3})	T (K)	B_{IMF} (nT)	IMF polarity
M1	420	60	1.2×10^5	18	Away
M2	380	60	2.0×10^5	15	Toward
M3	390	50	1.0×10^5	20	Away

The approximate values for the main WSA-ENLIL solar wind and IMF parameters during each of the three flybys are summarized in Table 1. Such parameters can provide a good starting place for magnetospheric modeling efforts (as argued above). This statement will be true as well for the Mercury orbital phase of the MESSENGER mission. A further point is that MESSENGER measurements of the IMF (and any available plasma observations) in the inner heliosphere provide helpful local "ground truth" for the WSA-ENLIL model calculations (Baker et al., 2009). Having *in situ* observations at ~0.3–0.4 AU heliocentric distance can be used with the model results to improve overall model performance. Such data–theory closure can lead to a better overall space-weather prediction capability at Earth for the operational WSA-ENLIL model (e.g., Baker et al., 2004).

One of the major puzzles of the three MESSENGER flybys is why we have seen essentially no energetic particles (i.e., with energy $E>30$ keV) in the Mercury magnetosphere (see Ho et al., this issue). Slavin et al. (2009, 2010) have shown evidence of strong magnetospheric energy loading of Mercury's magnetic tail due to solar wind coupling, especially during M3. Several events documented in the Magnetometer data suggest "substorm-like" behavior. Yet none of these events were accompanied by energetic particle bursts. A possible explanation is that the very benign solar wind driving conditions for all three flybys simply were not sufficient to produce strong energetic particle acceleration.

We look forward to future measurements of the Mercury system. The modeling shown here can provide useful contextual information for ground-based measurements. Beginning in March 2011 when MESSENGER will be inserted into orbit around Mercury, the spacecraft will be within the magnetosphere and magnetotail of the planet for extended periods of every orbit. Model results will provide continuous information about solar wind and IMF conditions that are driving magnetospheric dynamics and exosphere variability. The WSA-ENLIL time-dependent specifications and forecasts of solar wind parameters and IMF will provide valuable inputs to simulations of magnetospheric behavior during MESSENGER's orbital mission phase.

Acknowledgments

The MESSENGER project is supported by the NASA Discovery Program under contracts NASW-00002 to the Carnegie Institution of Washington and NAS5-97271 to the Johns Hopkins University

Applied Physics Laboratory. The modeling techniques described here were originally developed under the auspices of the National Science Foundation's Center for Integrated Space Weather Modeling.

References

Anderson, B.J., Acuña, M.H., Korth, H., Purucker, M.E., Johnson, C.L., Slavin, J.A., Solomon, S.C., McNutt Jr., R.L., 2008. The structure of Mercury's magnetic field from MESSENGER's first flyby. Science 321, 82–85. doi:10.1126/science.1159081.

Arge, C.N., Pizzo, V.J., 2000. Improvement in the prediction of SW conditions using near-real-time solar magnetic field updates. J. Geophys. Res. 105, 10,465–10,479.

Arge, C.N., Luhmann, J.G., Odstrcil, D., Schrijver, C.J., Li, Y., 2004. Stream structure and coronal sources of the solar wind during the May 12th, 1997 CME. J. Atmos. Solar-Terr. Phys. 66, 1295–1309.

Baker, D.N., Simpson, J.A., Eraker, J.H., 1986. A model of impulsive acceleration and transport of energetic particles in Mercury's magnetosphere. J. Geophys. Res. 91, 8742–8748. doi:10.1029/JA091iA08p08742.

Baker, D.N., Weigel, R.S., Rigler, E.J., McPherron, R.L., Vassiliadis, D., Arge, C.N., Siscoe, G.L., Spence, H.E., 2004. Sun-to-magnetosphere modeling: CISM forecast model development using linked empirical methods. J. Atmos. Solar-Terr. Phys. 66, 1491–1497. doi:10.1016/j.jastp.2004.04.011.

Baker, D.N., Odstrcil, D., Anderson, B.J., Arge, C.N., Benna, M., Gloeckler, G., Raines, J.M., Schriver, D., Slavin, J.A., Solomon, S.C., Killen, R.M., Zurbuchen, T.H., 2009. Space environment of Mercury at the time of the first MESSENGER flyby: solar wind and interplanetary magnetic field modeling of upstream conditions. J. Geophys. Res. 114, A10101. doi:10.1029/2009JA014287.

Benna, M., Anderson, B.J., Baker, D.N., Boardsen, S.A., Gloeckler, G., Gold, R.E., Ho, G.C., Killen, R.M., Korth, H., Krimigis, S.M., Purucker, M.E., McNutt Jr., R.L., Raines, J.M., McClintock, W.E., Sarantos, M., Slavin, J.A., Solomon, S.C., Zurbuchen, T.H., 2010. Modeling of the magnetosphere of Mercury at the time of the first MESSENGER flyby. Icarus 209, 3–10. doi:10.1016/j.icarus.2009.11.036.

de Toma, G., Gibson, S., Emery, B., Kozyra, J., 2010. Solar cycle 23: an unusual solar minimum? In: Maksmovic, M., Issautier, K., Meyer-Vernet, N., Moncuquet, M., Pantellini, F. (Eds.), Twelfth International Solar Wind Conference, AIP Conference Proceedings, vol. 1216, pp. 667–670, doi:10.1063/1.3395955.

Ho, G.C., Starr, R.D., Gold, R.E., Krimigis, S.M., Slavin, J.A., Baker, D.N., Anderson, B.J., McNutt, R.L., Jr., Nittler, L.R., Solomon, S.C. Observations of suprathermal electrons in Mercury's magnetosphere during the three MESSENGER flybys. Planet. Space Sci., this issue.

McComas, D.J., Ebert, R.W., Elliott, H.A., Goldstein, B.E., Gosling, J.T., Schwadron, N.A., Skoug, R.M., 2008. Weaker solar wind from the polar coronal holes and the whole Sun. Geophys. Res. Lett. 35, L18103. doi:10.1029/2008GL034896.

Odstrcil, D., Pizzo, V.J., Linker, J.A., Riley, P., Lionello, R., Mikic, Z., 2004. Initial coupling of coronal and heliospheric numerical magnetohydrodynamic codes. J. Atmos. Solar-Terr. Phys. 66, 1311–1320. doi:10.1016/j.jastp.2004.04.007.

Raines, J.M., Slavin, J.A., Zurbuchen, T.H., Gloeckler, G., Anderson, B.J., Korth, H., Krimigis, S.M., McNutt, R.L., Jr. MESSENGER observations of the plasma environment near Mercury. Planet. Space Sci., this issue.

Schatten, E.N., Wilcox, J.M., Ness, N.F., 1969. A model of interplanetary and coronal magnetic fields. Sol. Phys. 6, 442–455. doi:10.1007/BF00146478.

Schwenn, R., 1990. Large-scale structure of the interplanetary medium. In: Schwenn, R., Marsch, E. (Eds.), Physics of the Inner Heliosphere, 1. Large-Scale Phenomena. Springer-Verlag, Berlin, pp. 99–181.

Slavin, J.A., Acuña, M.H., Anderson, B.J., Baker, D.N., Benna, M., Gloeckler, G., Gold, R.E., Ho, G.C., Killen, R.M., Korth, H., Krimigis, S.M., McNutt Jr., R.L., Nittler, L.R., Raines, J.M., Schriver, D., Solomon, S.C., Starr, R.D., Trávníček, P., Zurbuchen, T.H., 2008. Mercury's magnetosphere after MESSENGER's first flyby. Science 321, 59–62. doi:10.1126/science.1159040.

Slavin, J.A., Acuña, M.H., Anderson, B.J., Baker, D.N., Benna, M., Boardsen, S.A., Gloeckler, G., Gold, R.E., Ho, G.C., Korth, H., Krimigis, S.M., McNutt Jr., R.L., Raines, J.M., Sarantos, M., Schriver, D., Solomon, S.C., Starr, R.D., Trávníček, P., Zurbuchen, T.H., 2009. MESSENGER observations of magnetic reconnection in Mercury's magnetosphere. Science 324, 606–610. doi:10.1126/science.1172011.

Slavin, J.A., Anderson, B.J., Baker, D.N., Benna, M., Boardsen, S.A., Gloeckler, G., Gold, R.E., Ho, G.C., Korth, H., Krimigis, S.M., McNutt Jr., R.L., Nittler, L.R., Raines, J.M., Sarantos, M., Schriver, D., Solomon, S.C., Starr, R.D., Trávníček, P., Zurbuchen, T.H., 2010. MESSENGER observations of extreme loading and unloading of Mercury's magnetic tail. Science 329, 665–668. doi:10.1126/science.1188067.

Smith, E.J., Balogh, A., 2008. Decrease in heliospheric magnetic flux in this solar minimum: recent Ulysses magnetic field observations. Geophys. Res. Lett. 35, L22103. doi:10.1029/2008GL035345.

Trávníček, P., Hellinger, P., Schriver, D., 2007. Structure of Mercury's magnetosphere for different pressure of the solar wind: three dimensional hybrid simulations. Geophys. Res. Lett. 34, L05104. doi:10.1029/2006GL028518.

Trávníček, P.M., Hellinger, P., Schriver, D., Hercik, D., Slavin, J.A., Anderson, B.J., 2009. Kinetic instabilities in Mercury's magnetosphere: three-dimensional simulation results. Geophys. Res. Lett. 36, L07104. doi:10.1029/2008GL036630.

Trávníček, P.M., Schriver, D., Hellinger, P., Hercik, D., Anderson, B.J., Sarantos, M., Slavin, J.A., 2010. Mercury's magnetosphere–solar wind interaction for northward and southward interplanetary magnetic field: hybrid simulation results. Icarus 209, 11–22. doi:10.1016/j.icarus.2010.01.008.

Vervack Jr., R.J., McClintock, W.E., Killen, R.M., Sprague, A.L., Anderson, B.J., Burger, M.H., Bradley, E.T., Mouawad, N., Solomon, S.C., Izenberg, N.R., 2010. Mercury's complex exosphere: results from MESSENGER's third flyby. Science 329, 672–675. doi:10.1126/science.1188572.

Wang, Y.-M., Sheeley Jr., N.R., 1992. On potential field models of the solar corona. Astrophys. J. 392, 310–319. doi:10.1086/171430.